designs

MDPI

Article

Quantum Deep Learning for Fast Switching of Full-Bridge Power Converters

Meysam Gheisarnejad * and Mohammad-Hassan Khooban

Department of Electrical and Computer Engineering, Aarhus University, 8200 Aarhus, Denmark
* Correspondence: me.gheisarnejad@gmail.com

Abstract: With the qualitative development of DC microgrids, the usage of different loads with unique conditions and features is now possible in electric power grids. Due to the negative impedance features of some loads, which are called constant power loads (CPLs), the control of DC power converters faces huge challenges from a stability point of view. Despite the significant advances in semiconductors, there is no upgrade in the control of gate drivers to exploit all potential of power electronic systems. In this paper, quantum computations are incorporated into artificial intelligence (AI) to stabilize a full-bridge (FB) DC-DC boost converter feeding CPL. Aiming to improve the bus voltage stabilization of the FB DC-DC boost converter, a quantum deep reinforcement learning (QDRL) control methodology is developed. By defining a reward function according to the specification of the FB power converter, the desired performance and control objectives are fulfilled. The main task of QDRL is to adjust the control coefficients embedded in the feedback controller to suppress the negative impedance effect resulting from deploying the CPLs. By deploying the potential advantages of quantum fundamentals, the deep reinforcement learning improved by quantum specifications will not only enhance the performance of the DRL algorithm on conventional processes but also advance related research areas such as quantum computing and AI. Unlike the basic quantum theory, which requires real quantum hardware, QDRL can be executed on classic computers. To examine the feasibility of the QDRL scheme, hardware-in-the-loop (HiL) examinations are conducted using the OPAL-RT. The comparison of the proposed controller with the classic state-of-the-art methodologies reveals the superiority and feasibility of QDRL-based control schemes in both the transient and steady-state conditions to other schemes. Analysis using various performance criteria, including the integral absolute error (IAE), integral time absolute error (ITAE), mean absolute error (MAE), and root mean square error (RMSE), demonstrates the dynamic improvement of the proposed scheme over sliding mode control (approximately 50%) and proportional integral control (approximately 100%).

Keywords: microgrid; full-bridge (FB) DC-DC boost converter; quantum deep reinforcement learning (QDRL); hardware-in-the-loop (HiL)

Citation: Gheisarnejad, M.; Khooban, M.-H. Quantum Deep Learning for Fast Switching of Full-Bridge Power Converters. *Designs* **2023**, *7*, 60. https://doi.org/10.3390/designs7030060

Academic Editor: Surender Reddy Salkuti

Received: 21 February 2023
Revised: 13 April 2023
Accepted: 21 April 2023
Published: 26 April 2023

1. Introduction and Preliminaries

With the vast penetration of non-conventional energy sources (photovoltaic (PV), hydropower, wind, geothermal, etc.) into modern power systems, the concept of integrating these technologies into microgrid (MG) form has drawn a lot of academic interest over the past 15 years [1–3]. These MGs' benefits include low-cost energy, high local resiliency, simple connection to power source units, and the growth of users who can be connected to them. Unlike AC microgrids (ACMGs), which face many challenges in the appearance of harmonics and reactive power and frequency synchronization, DC microgrids (DCMGs) are projected to play a particular role in power networks. Practically, various power interface converters and filters are embedded in the configuration of DCMGs to convert the energy of various types of sustainable sources for supplying DC/AC loads. Moreover, the distributed structure of integrated power systems can be created by paralleling power electronic interfaces [4,5].

Thanks to the excellent performance of wide-bandgap (WBG) semiconductors (e.g., the silicon carbide (4H-SiC) [6] and gallium nitride (GaN) [7,8]), it has become possible to achieve power converters with significant characteristics such as faster, fewer losses and more compactness. However, this potential performance can only be fulfilled if these technologies are incorporated into power converters that can handle them. Despite the remarkable advances at the device level by semiconductor manufacturers, a corresponding improvement has not occurred at the system level (control algorithms); as a result, a large portion of that potential is being lost.

Additionally, the configuration of loads might appear in the DC MGs with time-varying specifications during various operations of the system. As a result of such characteristics, higher standards for the system's stability are required from the control design perspective. The challenges of MG stabilization are heightened when its power source units supply the constant power loads (CPLs) [9–12]. In fact, such loads have negative impedance properties, which lead to a destabilization impact on DC MGs. To address this issue, robust H-infinity [13], backstepping-based sliding mode control (SMC) [14], offset-free composite model predictive control (MPC) [15,16], passivity-based control [17], etc., are utilized. For instance, Kaplan and Bodur [9] proposed a super-twisting-based second-order SMC (SOSMC) for stabilizing the output of the DC-DC buck converter in the presence of CPLs. The authors of ref. [18] developed a passivity-based control (PBC) to mitigate the destabilization effect of the power converters when supplying a CPL and a constant voltage in an MG system. Moreover, a nonlinear disturbance observer (NDO) was required to estimate line and load variation to ameliorate the performance of the designed PBC. Boukerdja et al. [13] developed H_∞ control at the source side of the buck converter to disappear the output fluctuations caused by the CPL at the load-side converter. Karami et al. [19] proposed a finite control set MPC (FCS-MPC) for DC-DC boost converters feeding nonlinear CPLs by minimizing a finite-prediction horizon objective function. These robust controllers have significantly contributed to the stability of power converters connected to CPLs, but a large part of the full potential of semiconductors still remains untapped. In ref. [20], Ullah et al. proposed a non-integer version of terminal sliding mode (TSMC) to suppress the destabilization impact resulting from constant power loads in DC boost converters. By adopting Lyapunov's theorem, a guaranteed stability performance was achieved with the non-integer TSMC.

Recently, the concept of the quantum process was incorporated into artificial intelligence with the aim of enhancing the essential functions of conventional deep neural networks (DNNs) [21,22]. In this regard, a quantum-inspired experience replay (QER) was developed [23] to ameliorate the training capability of deep reinforcement learning (DRL) without the need to adjust the hyperparameter. Quantum deep reinforcement learning (QDRL) was proposed in refs. [24,25], which combined the quantum superposition theory and deep RL algorithm. In QDRL, deep neural networks are used to predict the next systemic state to improve the quality of control commands. The simulation and experimental outcomes in various applications revealed that with the application of QDRL [23,26,27], a larger search space, quicker training, and more tradeoff between exploration and exploitation would be achievable in comparison with the classic version of DRL (CDRL) algorithms. Theoretically, it was demonstrated that for a wide class of learning problems, QDRL could produce quadratic progress in training effectiveness and significant feasibility in performance. The resilience of this QDRL algorithm was further illustrated by the generalization of this method to more effectively modify weights on favorable actions. Additionally, by adopting quantum computation, more control commands can be generated to provide accurate control [25,28].

In this paper, a robust control scheme is adopted by the training ability of the QDRL algorithm to stabilize the voltage output of a full-bride power converter feeding CPLs in the DCMGs architecture. In this application, a time-varying CPL is applied to the test system, which imposes the highest level of instability on the DCMG from an electronic power perspective. The main contributions of this work are provided as follows:

- A full-bridge boost converter feeding constant power loads is modeled in the form of microgrids. For this purpose, the average dynamics of the power interface system are provided.
- Quantum computation based on deep reinforcement learning is developed to control the FB power converter.
- Extensive examinations and comparative analyses are conducted to validate the efficiency of the proposed FB DC-DC power converter.
- HiL tests based on OPAL-RT are developed to test the feasibility of the proposed QDRL algorithm.

This article is organized as follows. In Section 2, the model of a full-bride power converter supplying CPL is illustrated. Then, all parts of the suggested control methodology are introduced in Section 3. Section 4 is devoted to the real-time examinations of the power electronic case study. The outcome of the work is concluded in Section 5.

2. Dynamic Model of Full Bridge Converter under CPL

The isolated full-bridge (FB) DC/DC converter is a practical and extensively adopted solution for isolated power converter systems. Full-bridge converters, when compared to other DC-DC converters, are suitable for integrated power systems where maximum voltage and maximum power are required. The feasible structure of the FB converter is depicted in Figure 1, which is constructed from a DC source, a boost converter, an isolated FB, and a constant power load [29,30].

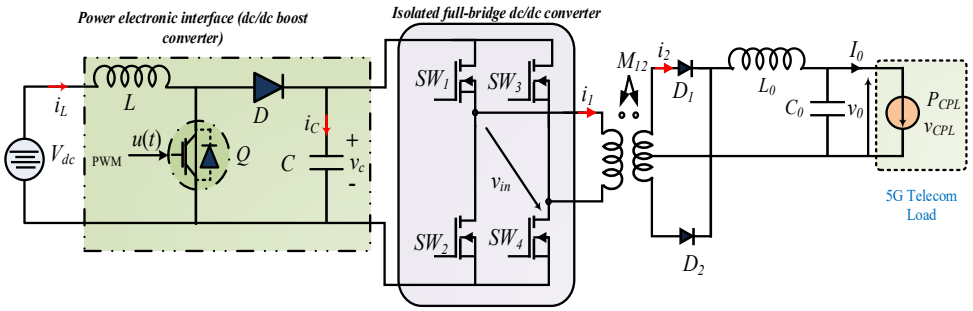

Figure 1. The configuration of the FB DC-DC converter connected to the CPL.

On the left side of the converter, a boost converter is configured, which steps up the input voltage (E or V_{dc}) to a higher level. In the context of MG, many generation units, such as fuel cells and photovoltaics, can be adopted as the input source. The main contribution of full-bridge FB is the transformation from a high-voltage bus to an intermediate level. The input voltage of the full-bridge converter should be set to 110 according to the reference voltage V_{ref}. Moreover, a transformer with an LC filter is implemented to transfer power instantaneously from the output of the FB converter to the external CPL load.

The dynamic equation of the CPL is given as [31]:

$$i_{CPL} = \left(\frac{P_{CPL}}{v_o}\right) \quad \forall v_{CPL} > \varepsilon, \tag{1}$$

where v_o and i_{CPL} denote the output voltage and current of the boost converter, respectively, and P_{CPL} is the CPL's power. The average model of the boost converter is formulated as [31]:

$$\frac{di_L}{dt} = \left(\frac{E}{L}\right) - \left(\frac{1-u}{L}\right)v_c, \tag{2}$$

$$\frac{dv_c}{dt} = \left(\frac{1-u}{L}\right)i_L - \left(\frac{P_{CPL}}{L}\right)v_c, \tag{3}$$

where v_c is the voltage of the inductance L and i_L is the current of the capacitor C in the boost converter.

3. Quantum Deep Reinforcement Learning for FB Power Converter

The control objective of the FB DC-DC converter is to regulate the output voltage in the structure of DC MG to its nominal voltage in the load bus. This work aims to stabilize the output voltage v_o under a time-varying CPL using quantum deep learning. For this purpose, a feedback controller with a structure of classic proportional-integral (PI) is adopted for the FB DC-DC system. The overall control structure of the FB DC-DC boost converter with the quantum process is depicted in Figure 2. According to Figure 2, quantum deep reinforcement learning is developed from three main components, including deep belief nets, reinforcement learning, and the quantum process. The deep neural network of QRL is trained in such a way that adjusts the gains of the established feedback controller (k_p and k_i) to reach a good control behavior so transient and steady-state conditions can be realized.

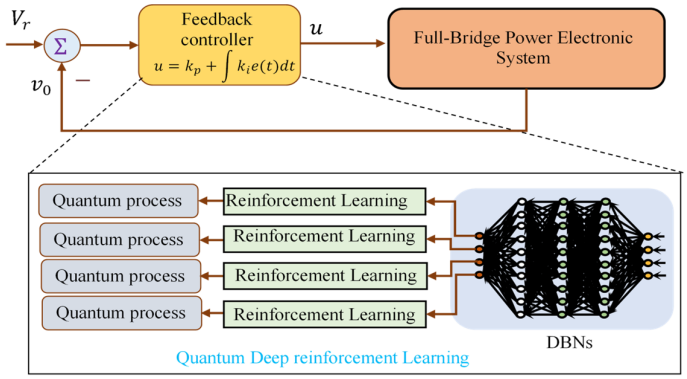

Figure 2. Overall diagram of QDRL-based feedback controller for stabilization of FB power converter.

3.1. Principal of RL

In every subordinate RL section of the quantum technique, a Q-value renovated procedure, a p-value renovated procedure, an action procedure, and quantum computation is included. In this structure, deep belief neural networks are adopted for prediction states O_i' to update the Q-value. In the p-value process, the p-value will be updated to reach the index of actions. The action will be chosen from activity space A. In the final step, the real action δ_i' will be generated by the quantum procedure.

Since the quantum deep RL includes a general RL architecture, it can ameliorate the efficiency and feasibility of power electronic equipment. The RL algorithm is made from four components consisting of states, actions of RL-agent, returns (rewards), and environment. The RL agent evaluates the environment, decides in accordance with the information acquired, and then communicates that choice to the system (action). According to the defined optimal policy, the agent will be trained in such a way that obtains more reward from the system. In the RL, the position of the current system is represented by the state that shows the agent's situation.

The control actions will be delivered to the system by updating the matrices of the Q-value:

$$\mathcal{Q}_{RL}(\mathcal{O}', \delta) = \mathcal{Q}_{RL}(\mathcal{O}, \delta) + \zeta_{RL} y, \tag{4}$$

$$y = P_{RL}(\mathcal{O}, \mathcal{O}', \delta) + \gamma_{RL} \max_{\delta \in A} \mathcal{Q}_{RL}(\mathcal{O}, \delta') - \mathcal{Q}_{RL}(\mathcal{O}, \delta), \tag{5}$$

and p-value [24]:

$$P_{RL}(\mathcal{O}', \delta) = \begin{cases} P_{RL}(\mathcal{O}, \delta) - \mu_{RL}(1 - P_{RL}(\mathcal{O}, \mathcal{O}', \delta)), \; if \; \delta' = \delta \\ P_{RL}(\mathcal{O}, \delta) - (1 - \mu_{RL}), \; if \; \delta' \neq \delta \end{cases}, \tag{6}$$

where ζ_{RL} is the learning factor, γ_{RL} is the discount factor, and μ_{RL} is the updated factor. It is assumed these coefficients are selected in the range of $[0,\ 1]$. Likewise, $\mathcal{O}$ denotes the current state, δ denotes the action, and $\mathcal{O}'$ denotes the predicted next state.

For the FB DC-DC converter, the reward function of QDRL is defined as:

$$R_{RL}(\mathcal{O},\mathcal{O}',\delta) = \begin{cases} \frac{\beta_2}{|E_{error}|} & if \quad E_{error} \leq 0.05 \\ -\beta_1|E_{error}|\ if & E_{error} > 0.05 \end{cases}, \tag{7}$$

where β_1 and β_2 are the constant factors and E_{error} is the difference between output voltage and its reference, i.e., $E_{error} = v_c(t) - V_{Ref}(t)$. According to the defined reward function, the QDRL algorithm tries to generate the action signals in such a way that mitigates the voltage fluctuations against the CPL.

3.2. Deep Belief Nets (BBNs) Based on Restricted Boltzmann Machines

Restricted Boltzmann machines (RBM) are a variant of Boltzmann machines that can be adopted to fine-tune deep belief nets (DBNs) using a greedy technique. Standard RBM are made from binary-valued visible and hidden units and comprise of a weight matrix $\boldsymbol{W}$ with a size of $m \times n$. In RBM, the relationship between the hidden layer (h_{ij}) and the visible layer (v_i) is represented by the weight component (w_{ij}). Moreover, some bias weights (offsets) are used, including b_{vi} and b_{hi} for v_i and h_i, respectively. Based on the biases and weights, the energy level of RBM of deep belief networks considering the test variables of $\boldsymbol{\theta} = \left\{\boldsymbol{W}^R,\ \boldsymbol{b}_v, \boldsymbol{b}_h\right\}$ is computed by [23,32]:

$$E(\boldsymbol{v},\boldsymbol{h};\boldsymbol{\theta}) = -\sum_{i=1}^{N_{Layer}} b_{vi}v_i - \sum_{j=1}^{N_{Hidden}} b_{hi}h_i - \sum_{i=1}^{N_{Layer}}\sum_{j=1}^{N_{Hidden}} v_i w_{ij}^R h_j, \tag{8}$$

where N_{Layer} and N_{Hidden} represent the hidden layers and hidden units, respectively. Additionally, $E(\boldsymbol{v},\boldsymbol{h};\boldsymbol{\theta})$ can be defined by the following notion:

$$E(\boldsymbol{v},\boldsymbol{h};\boldsymbol{\theta}) = -a^T\boldsymbol{v} - b^T\boldsymbol{h} - \boldsymbol{v}^T\boldsymbol{W}\boldsymbol{h}. \tag{9}$$

The following is the marginal probability for each potential hidden layer:

$$P(\boldsymbol{v};\theta) = \frac{\sum_h e^{-E(v,h;\theta)}}{\sum_{v,h} e^{-E(v,h;\theta)}}. \tag{10}$$

According to the Gibbs sampling theory, the probability distribution can be given as:

$$P\left(h_j = 1\middle|\boldsymbol{v};\boldsymbol{\theta}\right) = \frac{1}{1+e^{\left(-\left(b_j+\sum_i v_i w_{ij}^R\right)\right)}}, \tag{11}$$

$$P\left(v_j = 1\middle|\boldsymbol{h};\boldsymbol{\theta}\right) = \frac{1}{1+e^{\left(-\left(d_i+\sum_j v_j w_{ij}^R\right)\right)}}. \tag{12}$$

3.3. Quantum Computation

A quantum bit, also known as a qubit, is the fundamental data carrier in the quantum process, and it has the ability to exist in a super situation state of its eigenstates $|0\rangle$ and $|1\rangle$, which is defined by the following expression [23]:

$$|\psi\rangle = \gamma|0\rangle + \zeta|1\rangle, \tag{13}$$

where γ and ζ are complex constants qualifying $|\gamma|^2 + |\zeta|^2 = 1$.

The i^{th} action of DRL with the quantum process is generated as:

$$\delta'_{i,out} = \delta_k + \frac{\delta_{(k+1)} + \delta_{(k-1)}}{2}\left(q_i(\delta) - \frac{1}{2}\right), \tag{14}$$

where both the terms of $a_{(k+1)}$ and $a_{(k-1)}$ are considered the actions of set A, while the action δ_k is chosen from set A using the learning procedure of QDRL. Additionally, $q_i(\delta)$ denotes the output probability with the condition $0 \leq q_i(\delta) \leq 1$, which will be obtained by:

$$q_i(\delta) = |\delta_\delta^{N_A}\rangle = \sum_{\delta=00\ldots0}^{\overbrace{11\ldots1}^{K_Q}} C_\delta|\delta\rangle, \tag{15}$$

where $|C_a|^2$ is the likelihood that action $|\delta\rangle$ occurs among the sequence of $\left|\delta_\delta^{N_A}\right\rangle$; K_Q denotes the quantum bit count.

A detailed illustration of the quantum process based on DRL is depicted in Figure 3.

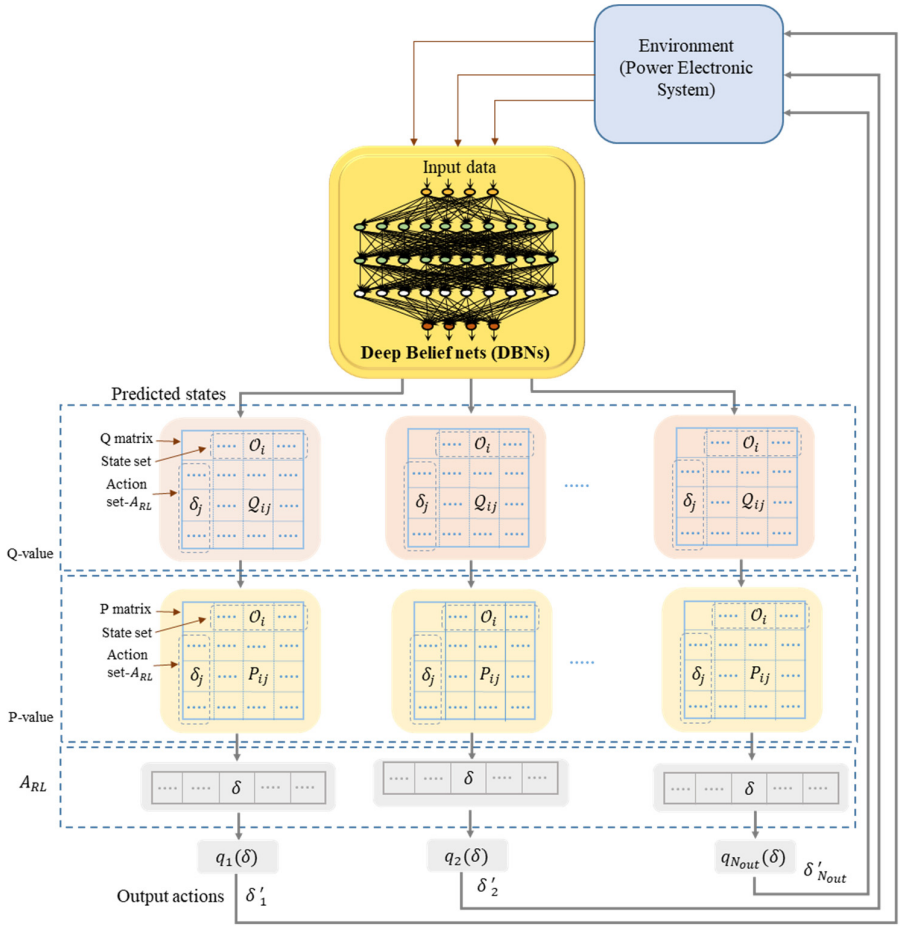

Figure 3. Schematic of quantum deep reinforcement learning.

4. Experimental Results

To demonstrate the robust performance and quick transient behavior of the proposed QDRL scheme, the real-time examinations of the FB system were accomplished using the OPAL-RT platform. A photograph of the OPAL-RT setup for the FB power converter is provided in Figure 4. The parameters of the FB power converter are shown in Table 1. The initial values of proportional and integral gains of the feedback controller were set as $k_{p0} = 0.3$ and $k_{i0} = 40$. The actions of QDRL were generated to adjust the gains of the feedback controller as $k_p = k_{p0} + \delta_p$ and $k_i = k_{i0} + \delta_i$. Here, the terms of δ_p and δ_i are the actions of QDRL used to adjust the coefficients of the feedback controller. The sliding mode control (SMC) and classic PI controller were also designed for the FB DC-DC boost converter for comparison purposes.

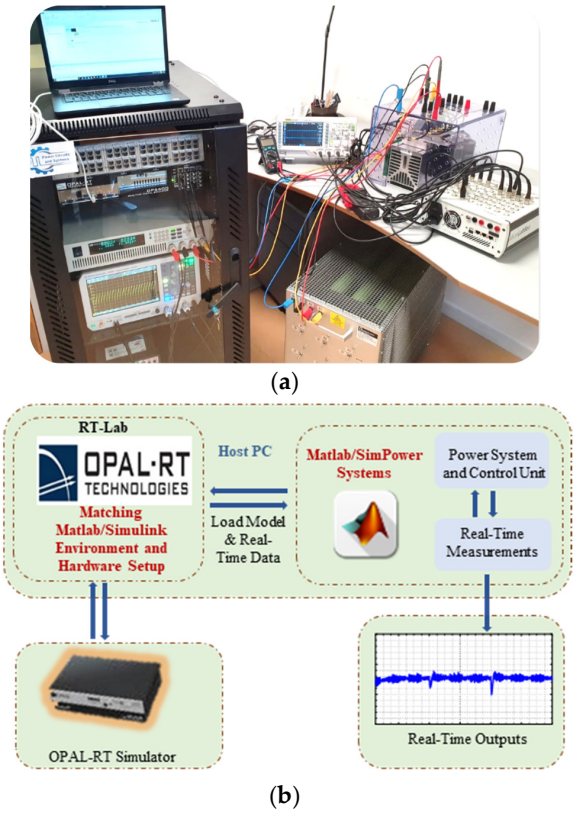

Figure 4. Illustration of a real-time testbed for the FB power converter: (**a**) photograph of OPAL-RT and (**b**) procedure of the real-time scheme.

Table 1. Parameters of the FB power converter.

Parameters	Values	Parameters	Values
Inductance of boost converter, L	1×10^{-3} H	Inductance of output filter, L_0	5.3×10^{-6} H
Capacitor of boost converter, C	0.9×10^{-3} F	Capacitor of output converter, C_0	2.09×10^{-6} F
Input voltage, E	48 V	Reference voltage, V_{ref}.	110 [V]

Scenario I: In the first step, a constant power load with the power of 300 [W] was connected to the full-bridge converter. The real-time responses of FB DC-DC converter in terms of capacitor voltage and output voltage (CPL's voltage) are provided in Figure 5a,b, respectively. From the real-time responses of the FB converter, it was revealed that, despite

the CPL imposing a high level of instability on the system, the designed controllers stabilized the output voltage at the desired range regarding the reference value. Moreover, a lower level of current fluctuations appeared using the proposed QDRL compared to the other designed controllers (SMC and classic PI controllers), as shown in Figure 6. Therefore, the proposed controller (realized by QDRL) improved the system stability and enhanced the system performance in terms of overshoot and settling time.

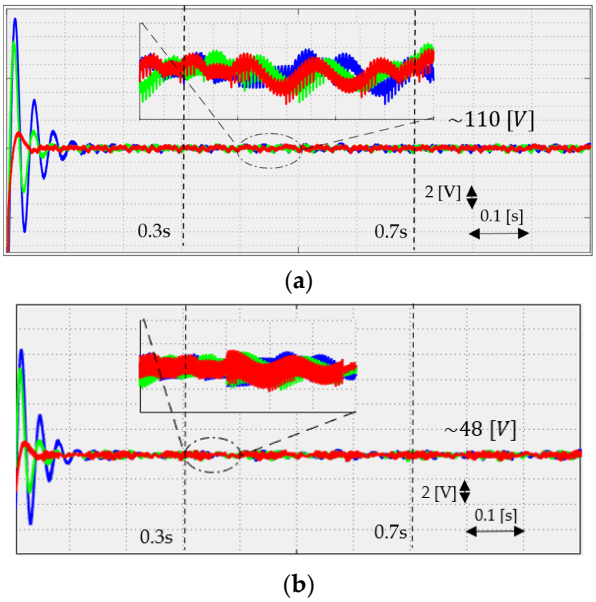

Figure 5. The voltage waveforms of the FB power converter under Scenario I: (**a**) capacitor voltage waveform and (**b**) CPL's voltage (PI controller shown in blue, SMC controller shown in green, and proposed technique shown in red).

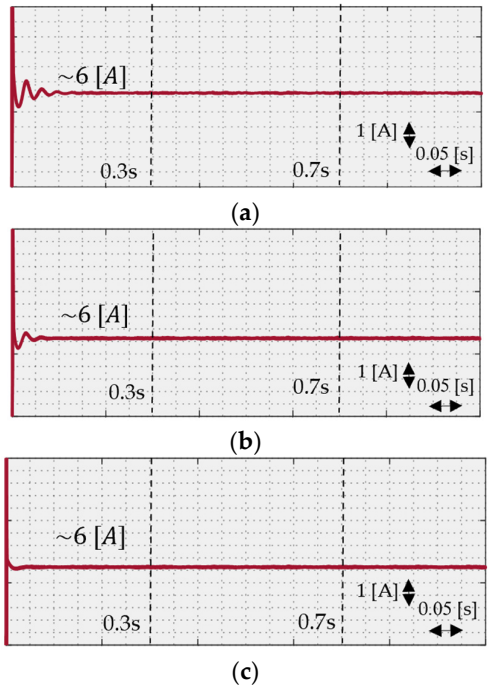

Figure 6. The inductor waveform of the FB power converter under Scenario I: (**a**) classic PI controller, (**b**) SMC, and (**c**) QDRL technique.

Scenario II: In this step, a time-varying CPL was connected to the full-bridge converter with the following changes.

$$P_{CPL} = \begin{cases} 300 & 0 < t \leq 0.3s \\ 550 & 0.3s < t \leq 0.7s \\ 450 & 0.7s < t \leq 1s \end{cases} \quad (16)$$

Figure 7 demonstrates the real-time outcome of the FB power converter, including the voltage bus and CPL's voltage under changes in the CPL's power [16]. The current signals of inductor for various controllers have been depicted in Figure 8. It is shown that when the CPL's power was changed during the experiment, the QDRL effectively stabilized the system outcomes. When the QDRL method was adopted, the settling time of the FB DC-DC power converter was significantly reduced in comparison with the two other ones. In addition, the system outcomes of the FB DC-DC power converter with the application of the proposed QDRL based on the controller experienced less overshoot than SMC and the classic PI controller.

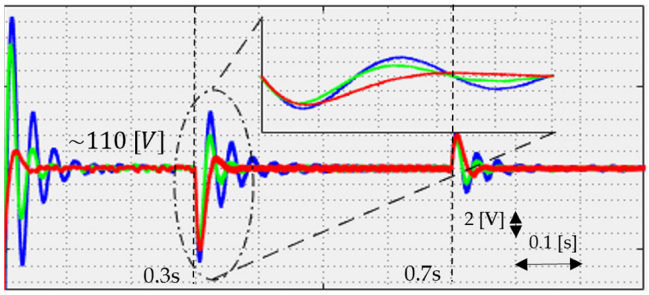

(**a**)

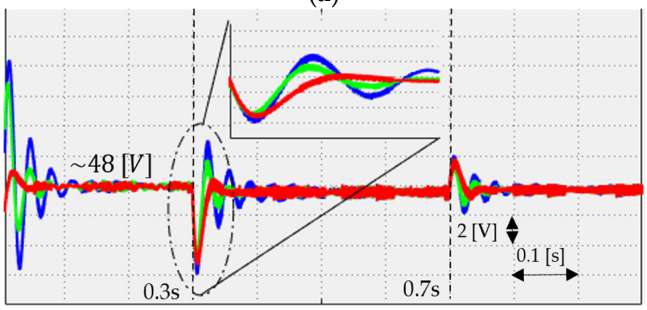

(**b**)

Figure 7. The voltage waveforms of the FB power converter under Scenario II: (**a**) capacitor voltage waveform and (**b**) CPL's voltage (PI controller shown in blue, SMC controller shown in green, and proposed technique shown in red).

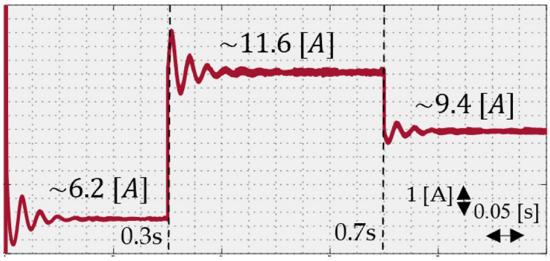

(**a**)

Figure 8. *Cont.*

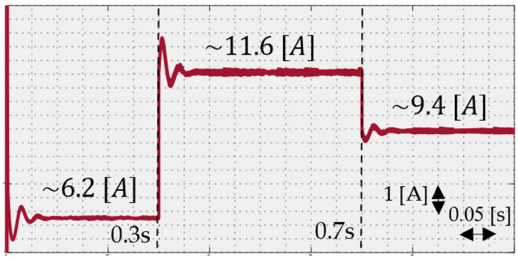

(**b**)

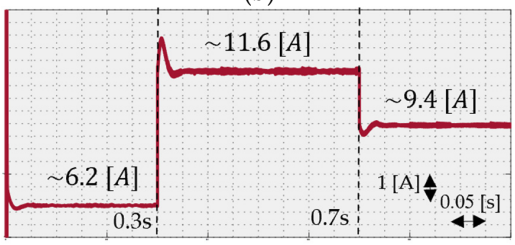

(**c**)

Figure 8. The current inductor waveform of the FB power converter under Scenario II: (**a**) classic PI controller, (**b**) SMC, and (**c**) QDRL technique.

For quantitative analysis of the FB power converter, various performance indices were considered to quantitatively evaluate the behavior of the designed controllers. For this purpose, the integral absolute error (IAE), integral time absolute error (ITAE), mean absolute error (MAE), and root mean square error (RMSE) were adopted as good options to demonstrate the superiority of the suggested QDRL technique. According to definitions of the above criteria, the best performance was obtained when the value of error was close to zero. The values of the performance index with the application of the PI controller, SMC, and QDRL control technique are shown in Table 2. For example, the values of IAE for case 1 with the proposed QDRL-based controller (IAE = 0.4889) were less than the SMC scheme (IAE = 0.6415) and classic PI controller (IAE = 0.8839). Additionally, for case 2, the values of IAE using the proposed QDRL-based controller (IAE = 0.6202) were smaller than the SMC scheme (IAE = 0.8343) and classic PI controller (IAE = 1.2599). According to these outcomes, the value of the performance index for IAE, ITAE, MAE, and RMSE for case 2 was more than for case 1, which indicates that the time-varying CPL's power imposes more of a destabilization effect than the ideal CPL. In addition, the proposed scheme (realized by the QDRL algorithm) obtained the lowest value of the performance index under ideal and time-varying CPL than the SMC scheme and classic PI controller.

Table 2. Values of performance criteria with the application of various controllers.

Performance Index	Classic PI Controller		SMC Scheme		Proposed QDRL Controller	
	Case1	**Case2**	**Case1**	**Case2**	**Case1**	**Case2**
IAE	0.8839	1.2599	0.6415	0.8343	0.4889	0.6202
ITSE	0.1108	0.2705	0.0942	0.1728	0.0775	0.1410
RMSE	4.6063	4.8075	4.4450	4.5547	4.1177	4.2382
MAE	0.8867	1.2625	0.6443	0.8370	0.4916	0.6229

Scenario III: In many cases, the voltage level of the DC source may change during the supply loads, which may affect the overall performance of the power electronic interfaces. Thus, in the final stage, the power's CPL and input source are changed simultaneously to examine the feasibility of the designed controller in the worst condition of the power converter system. For this purpose, the DC source voltage was reduced by 5% at $t = 0.3s$ from its nominal voltage ($t = 45.6s$) and was also increased by 5% at $t = 0.7s$ from its nominal voltage ($t = 50.4s$) (see Figure 9). The capacitor voltage waveforms of the FB

DC-DC power converter with the time-varying CPL and changes of DC source with the application of classic PI controller, SMC, and QDRL algorithm are depicted in Figure 10.

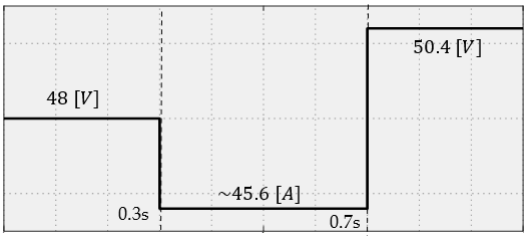

Figure 9. The curve of changes of input voltage.

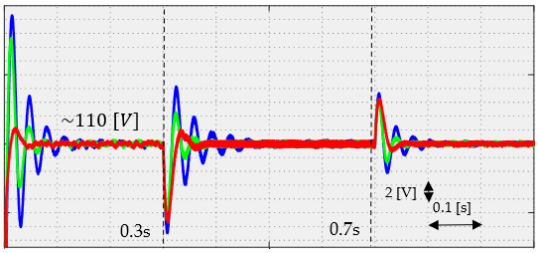

Figure 10. The waveforms of capacitor voltage of the FB DC-DC power converter under Scenario III (PI controller shown in blue, SMC controller shown in green, and proposed technique shown in red).

5. The Justification and Advantages of the Proposed Scheme

With the progress in the production of wide-bandgap (WBG) semiconductors, the performance of power interface systems has been remarkably enhanced at the device level. However, much of that potential is being lost since the system level (drivers, control algorithms, etc.) has not experienced matching advancement. This gap motivated the researchers to develop advanced control algorithms to exploit the maximum potential of semiconductors for improvement of the system performance. In particular, quantum computation can be adopted as a promising technique to control semiconductor devices with high-speed motor drivers, which was addressed in this paper.

The advantages of the QDRL technique for the power electronic case study are provided as follows:

(i) In comparison with model-based schemes (MPC, backstepping, SMC, etc.), which need model identification, a model-free QDRL learning scheme was developed to regulate the coefficients of the feedback controller.
(ii) Since the QDRL-based controller was developed in a model-free framework, the proposed QDRL scheme can be applied to a wide range of power electronic test systems.
(iii) In comparison to conventional controllers, which only have optimal performance at the operating condition, the proposed controller was adaptively adjusted by QDRL, which ensured the high efficiency of the FB DC-DC boost converter for all changes to the CPLs.
(iv) While ideal CPLs were often considered in previous works, in this study, a time-varying CPL was applied to evaluate the flexibility and effectiveness of the suggested QDRL-based controller.

6. Conclusions

In this paper, adaptive controller-based quantum computing was designed to suppress the effect of constant power loads in full-bridge converters in the form of a microgrid. By employing the training capability of the quantum deep reinforcement learning (QDRL) technique, the control parameters embedded in the feedback controller were adjusted appropriately and resulted in a robust controller with quick response. By using the error system in the reward function, the training of the QDRL algorithm was realized to stabilize

the output voltage of the FB DC-DC boost power converter feeding constant power load. To verify the efficiency of the suggested technique (realized based on the QDRL algorithm), real-time examinations with the OPAL-RT platform were conducted under two typical scenarios of microgrids. It was validated that despite the CPL being connected to the DC bus on the load side, the power electronic interface system operated in the ideal condition from a systematic point of view. In addition, the proportional-integral controller and sliding mode control were also designed and applied to the FB power converter for comparison purposes. The HiL outcomes of the QDRL technique-designed feedback controller showed a higher level of dynamic performance than other state-of-the-art techniques. In future work, a prototype of the FB power electronic system should be built to assess the feasibility of the proposed controller-based quantum theory from an experimental point of view. Additionally, the quantum principle can be adopted as a promising option to design model-predictive control for control output of the next generation of power electronic systems.

Author Contributions: Investigation, M.G.; methodology, M.G.; project administration, M.-H.K.; software, M.G.; validation, M.-H.K.; writing—original draft, M.G.; writing—review and editing, M.-H.K. All authors have read and agreed to the published version of the manuscript.

Funding: This research received no external funding.

Data Availability Statement: Not applicable.

Conflicts of Interest: The authors declare no conflict of interest.

Abbreviations

List of abbreviations

MG	Microgrid
DCMG	DC microgrid
ACMG	AC microgrid
WBG	Wide-bandgap
SIC	Silicon carbide
GAN	Gallium nitride
PI	Proportional-integral
SMC	Sliding mode control
MPC	Model predictive control
PBC	Passivity-based control
FCS-MPC	Finite control set MPC
DNN	Deep neural network
RBM	Restricted Boltzmann machine
CPL	Constant power load
PV	Photovoltaic
NDO	Nonlinear disturbance observer
DRL	Deep reinforcement learning
QDRL	Quantum deep reinforcement learning
QER	Quantum-inspired experience replay
WDRL	Quantum DRL
CDRL	Classic DRL
FB	Full-bridge
IAE	Integral absolute error
ITAE	Integral time absolute error
MAE	Mean absolute error
RMSE	Root mean square error

List of symbols

v_o	Output voltage
$V_{Ref}(t)$	Reference of output voltage
i_{CPL}	Current of CPL
P_{CPL}	Power of CPL
ζ_{RL}	Learning factor of _Q-value
γ_{RL}	Discount factor of Q-value
μ_{RL}	Updated factor of *p*-value
A	Set of action space
$\mathcal{O}$	Current state
δ	Action
$\mathcal{O}'$	Predicted next state
β_1, β_2	Constant factors of the reward function
E_{error}	Voltage error
$\boldsymbol{W}$	Weight matrix of RBM
h_{ij}	Hidden layer
v_i	Visible layer
w_{ij}	Weight component
b_{vi}	Bias weights of visible layer
b_{hi}	Bias weights of hidden layer
N_{Layer}	Number of hidden layers
N_{Hidden}	Number of hidden units
q_i	Output probability of QDRL
K_Q	Quantum bit count

References

1. Pérez-Lombard, L.; Ortiz, J.; Pout, C. A review on buildings energy consumption information. *Energy Build.* **2008**, *40*, 394–398.
2. Ansari, S.; Chandel, A.; Tariq, M. A Comprehensive Review on Power Converters Control and Control Strategies of AC/DC Microgrid. *IEEE Access* **2020**, *9*, 17998–18015.
3. San, G.; Zhang, W.; Guo, X.; Hua, C.; Xin, H.; Blaabjerg, F. Large-disturbance stability for power-converter-dominated microgrid: A review. *Renew. Sustain. Energy Rev.* **2020**, *127*, 109859.
4. Xu, L.; Guerrero, J.M.; Lashab, A.; Wei, B.; Bazmohammadi, N.; Vasquez, J.C.; Abusorrah, A. A Review of DC Shipboard Microgrids—Part I: Power Architectures, Energy Storage, and Power Converters. *IEEE Trans. Power Electron.* **2021**, *37*, 5155–5172.
5. Hu, J.; Shan, Y.; Cheng, K.W.; Islam, S. Overview of power converter control in microgrids—Challenges, advances, and future trends. *IEEE Trans. Power Electron.* **2022**, *37*, 9907–9922.
6. Bencherif, H.; Dehimi, L.; Pezzimenti, F.; De Martino, G.; Della Corte, F.G. Multiobjective optimization of design of 4H-SiC power MOSFETs for specific applications. *J. Electron. Mater.* **2019**, *48*, 3871–3880.
7. Jon, A.A.; Kessy, L.P.; Dominik, B.; Johann, W.K.; Matthias, J.K. Experimental characterization of silicon and gallium nitride 200 V power semiconductors for modular/multi-level converters using advanced measurement techniques. *IEEE J. Emerg. Sel. Top. Power Electron.* **2019**, *8*, 2238–2254.
8. Jin, W.; Lee, A.T.L.; Tan, S.C.; Hui, S.Y. A gallium nitride (GaN)-based single-inductor multiple-output (SIMO) inverter with multi-frequency AC outputs. *IEEE Trans. Power Electron.* **2019**, *34*, 10856–10873.
9. Kaplan, O.; Bodur, F. Second-order sliding mode controller design of buck converter with constant power load. *Int. J. Control* **2022**, *96*, 1210–1226.
10. Marcillo, K.E.L.; Guingla, D.A.P.; Barra, W.; De Medeiros, R.L.P.; Rocha, E.M.; Benavides, D.A.V.; Nogueira, F.G. Interval robust controller to minimize oscillations effects caused by constant power load in a DC multi-converter buck-buck system. *IEEE Access* **2019**, *7*, 26324–26342.
11. Khooban, M.H. Smartenance DC-DC On-Board Power Converters. *IEEE Trans. Circuits Syst. II Express Briefs* **2022**, *70*, 191–195.
12. Farsizadeh, H.; Gheisarnejad, M.; Mosayebi, M.; Rafiei, M.; Khooban, M.H. An Intelligent and Fast Controller for DC/DC Converter Feeding CPL in a DC Microgrid. *IEEE Trans. Circuits Syst. II Express Briefs* **2019**, *67*, 1104–1108.
13. Boukerdja, M.; Chouder, A.; Hassaine, L.; Bouamama, B.O.; Issa, W.; Louassaa, K. H∞ based control of a DC/DC buck converter feeding a constant power load in uncertain DC microgrid system. *ISA Trans.* **2020**, *105*, 278–295.
14. Alipour, M.; Zarei, J.; Razavi-Far, R.; Saif, M.; Mijatovic, N.; Dragicevic, T. Observer-based backstepping sliding mode control design for microgrids feeding a constant power load. *IEEE Trans. Ind. Electron.* **2022**, *70*, 465–473.
15. Xu, Q.; Yan, Y.; Zhang, C.; Dragicevic, T.; Blaabjerg, F. An offset-free composite model predictive control strategy for DC/DC buck converter feeding constant power loads. *IEEE Trans. Power Electron.* **2019**, *35*, 5331–5342.

16. Gheisarnejad, M.; Mohammadzadeh, A.; Khooban, M.-H. Model Predictive Control Based Type-3 Fuzzy Estimator for Voltage Stabilization of DC Power Converters. *IEEE Trans. Ind. Electron.* **2021**, *69*, 13849–13858.
17. He, W.; Namazi, M.M.; Koofigar, H.R.; Amirian, M.A.; Blaabjerg, F. Stabilization of DC–DC buck converter with unknown constant power load via passivity-based control plus proportion-integration. *IET Power Electron.* **2021**, *14*, 2597–2609.
18. Hassan, M.A.; Su, C.-L.; Chen, F.-Z.; Lo, K.-Y. Adaptive Passivity-Based Control of a DC–DC Boost Power Converter Supplying Constant Power and Constant Voltage Loads. *IEEE Trans. Ind. Electron.* **2021**, *69*, 6204–6214.
19. Karami, Z.; Shafiee, Q.; Sahoo, S.; Yaribeygi, M.; Bevrani, H.; Dragicevic, T. Hybrid model predictive control of DC–DC boost converters with constant power load. *IEEE Trans. Energy Convers.* **2020**, *36*, 1347–1356.
20. Ullah, N.; Asghar, M.; Khattak, A.; Rafiq, M.M. Comparison of integer and fractional order robust controllers for DC/DC converter feeding constant power load in a DC microgrid. *Sustain. Energy Grids Netw.* **2017**, *12*, 1–9.
21. Huang, H.-Y.; Broughton, M.; Mohseni, M.; Babbush, R.; Boixo, S.; Neven, H.; McClean, J.R. Power of data in quantum machine learning. *Nat. Commun.* **2021**, *12*, 2631.
22. Wu, S.L.; Yoo, S. Challenges and opportunities in quantum machine learning for high-energy physics. *Nat. Rev. Phys.* **2022**, *4*, 143–144.
23. Wei, Q.; Ma, H.; Chen, C.; Dong, D. Deep reinforcement learning with quantum-inspired experience replay. *IEEE Trans. Cybern.* **2021**, *52*, 9326–9338.
24. Yin, L.; Chen, L.; Liu, D.; Huang, X.; Gao, F. Quantum deep reinforcement learning for rotor side converter control of double-fed induction generator-based wind turbines. *Eng. Appl. Artif. Intell.* **2021**, *106*, 104451.
25. Chellaswamy, C.; Geetha, T.; Selvan, P.T.; Arunkumar, A. 6-phase DFIG for wind energy conversion system: A hybrid approach. *Sustain. Energy Technol. Assess.* **2022**, *53*, 102497.
26. Li, J.-A.; Dong, D.; Wei, Z.; Liu, Y.; Pan, Y.; Nori, F.; Zhang, X. Quantum reinforcement learning during human decision-making. *Nat. Hum. Behav.* **2020**, *4*, 294–307.
27. Yan, R.; Wang, Y.; Xu, Y.; Dai, J. A Multiagent Quantum Deep Reinforcement Learning Method for Distributed Frequency Control of Islanded Microgrids. *IEEE Trans. Control Netw. Syst.* **2022**, *9*, 1622–1632.
28. Baum, Y.; Amico, M.; Howell, S.; Hush, M.; Liuzzi, M.; Mundada, P.; Merkh, T.; Carvalho, A.R.; Biercuk, M.J. Experimental deep reinforcement learning for error-robust gate-set design on a superconducting quantum computer. *PRX Quantum* **2021**, *2*, 040324.
29. Aghdam, M.H.; Thiringer, T. Comparison of SiC and Si power semiconductor devices to be used in 2.5 kW DC/DC converter. In Proceedings of the 2009 International Conference on Power Electronics and Drive Systems (PEDS), Taipei, Taiwan, 2–5 November 2009; pp. 1035–1040.
30. Gheisarnejad, M.; Mohammadzadeh, A.; Farsizadeh, H.; Khooban, M.-H. Stabilization of 5G telecom converter-based deep type-3 fuzzy machine learning control for telecom applications. *IEEE Trans. Circuits Syst. II Express Briefs* **2021**, *69*, 544–548.
31. Xu, Q.; Zhang, C.; Wen, C.; Wang, P. A novel composite nonlinear controller for stabilization of constant power load in DC microgrid. *IEEE Trans. Smart Grid* **2017**, *10*, 752–761.
32. Wang, G.; Qiao, J.; Bi, J.; Jia, Q.-S.; Zhou, M. An adaptive deep belief network with sparse restricted Boltzmann machines. *IEEE Trans. Neural Netw. Learn. Syst.* **2019**, *31*, 4217–4228.